Effect of laser shock peening on residual stress and fatigue life of clad 2024 aluminium sheet containing scribe defects

Journal Item

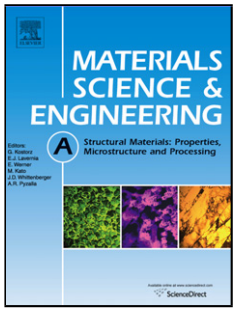

Title: Effect of laser shock peening on residual stress and fatigue life of clad 2024 aluminium sheet containing scribe defects

Authors: M. Dorman, M.B. Toparli, N. Smyth, A. Cini, M.E. Fitzpatrick, P.E. Irving

PII: S0921-5093(12)00488-1
DOI: doi:10.1016/j.msea.2012.04.002
Reference: MSA 28483

To appear in: *Materials Science and Engineering A*

Received date: 22-9-2011
Revised date: 31-3-2012
Accepted date: 2-4-2012

Please cite this article as: M. Dorman, M.B. Toparli, N. Smyth, A. Cini, M.E. Fitzpatrick, P.E. Irving, Effect of laser shock peening on residual stress and fatigue life of clad 2024 aluminium sheet containing scribe defects, *Materials Science & Engineering A* (2010), doi:10.1016/j.msea.2012.04.002

Effect of laser shock peening on residual stress and fatigue life of clad 2024 aluminium sheet containing scribe defects

M. Dorman[a], M. B. Toparli[b], N. Smyth[c], A. Cini[c], M. E. Fitzpatrick[b], P. E. Irving[c*]

a Department of Aerospace Engineering, Cranfield University, Cranfield, Beds, MK43 0AL, UK,
(now at RAAF, Victoria, Australia),
b Materials Engineering, The Open University, Walton Hall, Milton Keynes MK7 6AA, UK
c Departtment of Materials, Cranfield University, Cranfield, Beds, MK43 0AL, UK;
*Corresponding author p.e.irving@cranfield.ac.uk; 44-(0)-1234-754129; fax 44-(0)-1234-750875

Key words: Laser peening; aluminium sheet; fatigue, residual stresses, crack growth

Abstract

Laser peening at a range of power densities has been applied to 2-mm-thick sheets of 2024 T351 aluminium. The induced residual stress field was measured using incremental hole drilling and synchrotron X-ray diffraction techniques. Fatigue samples were subjected to identical laser peening treatments followed by scribing at the peen location to introduce stress concentrations, after which they were fatigue tested. The residual stresses were found to be non-biaxial: orthogonal to the peen line they were tensile at the surface, moving into the desired compression with increased depth. Regions of peen spot overlap were associated with large compression strains; the centre of the peen spot remaining tensile. Fatigue lives showed moderate improvement over the life of unpeened samples for 50 μm deep scribes, and slight improvement for samples with 150 μm scribes. Use of the residual stress intensity K_{resid} approach to calculate fatigue life improvement arising from peening was unsuccessful at predicting the relative effects of the different peening treatments. Possible reasons for this are explored.

1 Introduction

Laser peening is a comparatively recently-developed technique for surface treatment of metal components and structures. In laser peening treatment the sample is subjected to short duration pulses from a laser which generates a confined plasma on the surface. The plasma has an extremely high pressure (up to 10 GPa) [1] which is in turn transmitted into the sample via shock waves which plastically deform the near-surface region. The local plastic deformation causes compressive residual stresses to develop at the surface.

Over the past decade there have been many published investigations to measure the residual stress fields produced after laser peening, and to document the improvements, particularly in fatigue durability and strength, that can be produced. It is concluded that residual stress fields from laser peening are larger and extend to a greater depth in the components than is found with traditional mechanical shot peening, and that the fatigue strength and durability of samples subjected to laser treatment are superior to those produced by mechanical peening. There appear to be two variants of the laser peening treatment. One variant [2-4] uses a spot size of approximately 1 mm diameter or less,

and pulse frequencies up to 10 Hz. The other uses spot sizes of 3-10 mm diameter and pulse frequencies of the order of 0.1-0.2 Hz [5-7].

In order to treat samples and components representative of engineering use the peening treatment needs to be applied over areas considerably greater than the spot size. This is accomplished by following a procedure in which sequences of peened spots are laid down in a raster pattern. The overlap between the spots in a row and between rows of spots can be varied from a few % up to a full 100% or greater (see figure (1)).

A number of workers (e.g. [8-10]) have developed elastic-plastic finite element models based on the effects of different parameters on the pressure pulse peak and the influence that this has on plastic deformation of the surface layers, for prediction of residual stresses in laser peening. Parameters which influence the pressure peak and residual stresses are the power density of the pulses, the spot size, the pulse duration and the degree of overlap in the raster sequence. In work by Ling *et al.* [5], modelling laser peening of 304 stainless steel, increasing power density from 3.4 to 6.5 GW/cm^2 increased peak residual stresses from –150 MPa to –750 MPa. Spot size changes from 1-3 mm diameter produced significant changes in the depth at which the peak occurred. Increasing the degree of spot overlap from zero to 100% increased residual stresses compressive peak from –250 to –350 MPa.

Residual stresses and fatigue performance produced by laser peening have been measured in steels [2, 5, 8] titanium alloys [7, 9, 11, 12] and aluminium alloys [1, 3, 4, 13-23], and broadly similar conclusions are found for each. The maximum compressive residual stresses are generally of the order of 0.5-0.6 σ_y, the yield stress of the treated material, and extend 1-2 mm into the depth of the sample. There are reports [12] that peening with repeated overlaps at a pulse density of 2,500 pulses/cm^2 with pulses of 1.5 mm diameter can produce compressive stresses up to 1600 MPa in a 6061 aluminium alloy with a yield strength of 250-300 MPa. These figures are obviously significantly in excess of the nominal yield strength of the alloy. Fatigue performance is invariably enhanced by the laser peening treatment: fatigue endurance as measured by S-N curves is significantly improved, and fatigue crack growth rates are reduced.

Measuring the effects of the peen residual stress field on fatigue strength requires a degree of experimental ingenuity, as the compressive residual stress field will be balanced by tensile residual stresses on the surface adjacent to the peened area and also in the interior of the sample. Unless the compressive residual stresses are located in regions of the sample with greater applied stress than the regions containing tensile residual stress, fatigue failure will occur preferentially in the regions with tensile stresses and the full potential of the laser peen improvement will not be realised. Some researchers overcame this problem using stress concentrators in the form of notches and holes in the region of compressive residual stress [3]; others – e.g. Luong and Hill [18] – used trapezoidal samples tested in 4-point bending in which the region of greatest alternating fatigue stress was the smallest side of the trapezoid and this was treated with peening; the balancing tensile regions being located at other regions of the sample with reduced alternating stresses.

There have been some investigations and theoretical predictions of residual stresses and fatigue performance of peened thin (<2 mm) sheet material [5, 10, 21]; all other investigations of the fatigue performance of peened components have used samples of at

least 5-6 mm thick. Residual stresses in thin sheet are predicted [5] to be significantly different from those found in thick material, and in addition, there may be other effects associated with stress relaxation and sample distortion. Thin sheets have also been used to study mechanical property and microstructural changes after laser peening [22, 24, 25].

In order to investigate the benefits of laser peening in thin sheet material, this paper reports on an investigation into fatigue performance and residual stress development in 2 mm thick 2024 T351 clad aluminium alloy treated with laser peening. Fatigue cracks were encouraged to develop in the peened region by use of scribes with a high stress concentration located in the peened area.

2. Materials and Experimental techniques

2.1 Material

The material chosen for the study was 2-mm-thick clad 2024 T 351 aluminium sheet. Typical mechanical properties of the bulk material are shown in table I.

Table I.

Typical mechanical properties of clad 2024 T351 [26]

Material	Young modulus E / MPa	Yield stress $\sigma_{0.2}$ / MPa	Ultimate stress σ_u / MPa	Elongation at fracture / %
Al 2024-T351	72000	360	481	19

The clad layer is of soft unalloyed aluminium with an estimated proof strength of approximately 120 MPa. Metallographic sections of the alloy show that the clad layer is about 70 μm thick. Figure 2a shows the clad layer as the light etching constituent on the outer surfaces of the sheet. Figure 2b shows that the substrate grain structure is a typical "pancake" structure, with grain diameters in the longitudinal direction of 100-200 μm and in the through thickness direction of 20-30 μm.

In order to remove potential complexities associated with the clad layer on the residual stress generation, some samples were prepared with the clad layer removed by chemical milling. These samples therefore had a slightly reduced thickness of 1.8 mm.

2.2 Fatigue test sample design

The fatigue test samples were dogbone shaped as shown in figure 3, with an overall length of 400 mm and a width of 80 mm at the minimum diameter. The fatigue performance of this sample geometry has been studied extensively in previous research exploring the fatigue performance of 2024 T351 [27]. In order to initiate a fatigue crack at a defined location, a scribe perpendicular to the longitudinal axis of the sample was inserted at the point of minimum diameter using a diamond-tipped tool with a 5 μm root radius. The scratches or scribes were of accurately controlled dimensions and were either 50 or 150 μm deep ± 3 μm extending over the entire minimum sample width. Procedures for creating the scribes are described in detail in [28]. A typical transverse section of a 50 μm scribe can be seen in figure 4.

2.3 Procedures for laser peening

The trial peening was performed by the Metal Improvement Company, Earby, UK, with a range of peen conditions and geometries. In all cases, a sequence of pulses was applied to the plate, either as a single line or a small grid. In all cases there was an overlap of 5% between each spot. The effect of power density, acoustic damping and the use of ablative tape on the residual stress field extending from the sample surface into the thickness of the sheet was systematically explored. The power density of the spots was varied from 0.5 GW/cm^2 to 4 GW/cm^2. The pulse duration was 18 ns. Full details of the peen conditions for each sample are provided in the results section.

2.4 Residual stress measurement

Two methods were applied for the analysis of the residual stress in the materials: incremental hole drilling and synchrotron X-ray diffraction. Synchrotron X-ray time is in high demand and therefore in this project we targeted its use to where high-resolution spatial maps were required. For comparison between different peen parameters, incremental hole drilling provides rapid in-house data acquisition, and we applied this to evaluate the peen profiles through depth.

2.4.1 Incremental hole drilling

Residual stress measurements via incremental hole drilling were performed using a system developed by Stresscraft, UK, with strain relaxation being monitored by Measurements Group gauges in a standard three-gauge rosette (two gauges at 90˚ with a third at 45˚). The measurements were performed according to the guidance given in the UK NPL Good Practice Guide [29]. A hole of nominal diameter 2 mm was introduced by orbital hole drilling, and the final diameter of the hole was measured accurately (to 0.01 mm) after drilling. The relaxed strains were recorded at 16 depth increments: four increments of 32 μm, four increments of 64 μm, and eight increments of 128 μm, to a total hole depth of just over 1.4 mm. Increasing the increment size with depth counters the reduced sensitivity of the surface gauges as the hole depth increases [29]. Strains from the three gauges were recorded at each drill increment.

The results were interpreted using the integral method developed by Schajer [29, 30], with Stresscraft RS INT software version 5.1.2. The integral method is an extension to standard hole drilling analyses which allow for calculation only of stresses that are invariant with depth. A Young's modulus of 72 GPa and Poisson's ratio of 0.3 were used in calculating the stresses. The method provides a calculated stress profile up to ~1 mm in depth.

A total hole depth of 1.4 mm is not generally advisable for a sample of 2 mm thickness, as the hole depth should ideally be less than one-third of the specimen thickness. In order to mitigate any errors, the sample was adhesively bonded to a thick backing plate to provide additional restraint against distortion during drilling. The results from incremental hole drilling were also verified using a proprietary thin-plate correction at Stresscraft Ltd, and there was seen to be little significant change in the results.

2.4.2 Synchrotron X-ray diffraction

Synchrotron X-ray diffraction was performed on the ID31 beam line at the European Synchrotron Radiation Facility (ESRF). An incident beam energy of ~60 keV was used,

which corresponds to an X-ray wavelength of 0.21 Å and gave a diffraction angle at $2\theta \sim 9.9^{\circ}$. The {311} lattice planes were selected, as in fcc materials the elastic response of this plane is closest to that of the macroscopic elastic response of the material [31]. Shifts in position of the Bragg diffraction peak can be related to the internal strain ε *via*:

$$\varepsilon = -\cot\theta \, \Delta\theta \qquad (1)$$

where $\Delta\theta$ is the shift in peak position and θ is the diffraction angle in the strain-free condition.

The sample was mounted on an *xyz* translation table to enable mapping of the strains within the sample in and around the peened area. The ID31 instrument has a set of analyser crystals between the sample and the detector which ensures that near-surface measurements can be obtained without problems of spurious shifts in the diffraction peak owing to partial filling of the diffraction gauge volume.

2.4.3 Fatigue testing

Tension-tension fatigue tests were conducted in load control on a 100 kN servo hydraulic fatigue machine. The test frequency was 10 Hz, and the load ratio R = 0.1. The maximum stress in the fatigue cycle was 200 MPa for all the tests. Tests were performed in the unscribed and unpeened, scribed and unpeened, and in the scribed and peened conditions. For the latter tests scribing took place after peening. After the fatigue tests were complete the fracture surfaces were examined optically and in the scanning electron microscope.

3 Results

3.1 Surface relief and hardness of the peen spot array

The peening caused visible modification to the surface of the plates, with the individual peen spots being clearly visible. Figure 5a shows the optical appearance and figure 5b shows the surface profile, measured using a contour measurement machine, of three peen spots from a line peened at 3 GW/cm^2. The outline of each location of the laser pulse can be seen together with the 5% overlap region. The surface hardness profile after laser peening is shown in figure 6. There is clear evidence of hardening in the area of reduced height marking the peened region. There is no clear link between the hardness contours within the recess and the surface relief there. Outside the recess the area of raised height is softer than the area of reduced height.

3.2 Effects of laser peen conditions on residual stress field

All samples were treated with acoustic damping and ablative tape. Quantitatively the stress values obtained depended greatly on the peening conditions. A consistent result was that when the peening pattern was a single line of peened spots, the residual stress induced was more compressive parallel than perpendicular to the line axis. A single line was used in order to localise the benefit of the peening within the samples tested, though this result has wider implications for the application of peening in small patches.

Typical profiles of residual stress as a function of depth produced by a peening power density of 3.0 GW/cm^2 are shown in figure 7 for stresses parallel with the long direction of the peen spot array (σ_1) and perpendicular to it (σ_2). Measurements were made by incremental hole drilling, with the hole centred at the centre of a peen spot within the array. The spot size in this case was 8×8 mm^2. The stress field is partially biaxial with the σ_2 stresses perpendicular to the peen line always more tensile than the σ_1 stresses parallel to it, irrespective of whether the overall field was in tension or compression. Stresses at or near the surface were invariably in tension with stresses in both directions moving into compression with increased depth, reaching a compression peak at 100-300 μm beneath the surface, then moving back towards tension at greater depths. It can be seen that there is no great effect of the presence of the clad layer on the residual stress profiles obtained.

The effect of power density on residual stress values was studied for power density values between 0.5 and 4.0 GW/cm^2. Increased power density increased the compressive maximum in both stress components parallel and perpendicular to the peen line. This is shown in figure 8, where the peak compressive stress perpendicular to the line of peening increases from –7 MPa to –70 MPa with a power density increase from 0.5-3 GW/cm^2. Parallel to the peening line the stresses at the compression maximum increase from –80 MPa at 0.5 GW/cm^2 to –130 MPa at 3 GW/cm^2. At 4 GW/cm^2 there was a slight reduction in compression stress parallel with the peen line and a much larger reduction to almost zero in stresses perpendicular to the peen line. The depth profile of residual stress produced by the 4.0 GW/cm^2 pulses are similar to those produced by pulses of smaller energy density, though the level of biaxiality is least, and there is now significant (approaching 100 MPa) tensile residual stress at the surface of the sheet.
Increasing the laser power density also increased the depth of the compressive maximum in stress. This is shown in Table II. The depth of the compressive maximum stress increases from 100 μm at 0.5 GW/cm^2 to 450 μm for the 4 GW/cm^2 pulse.

Table II.

Effect of laser power density on the depth of the compression maximum stress perpendicular to peen line

Laser power density / GW cm^{-2}	Depth of peak compressive stress / μm
0.5	100
1	180
3	315
4	450

At all power densities the residual stresses perpendicular to the peening line were small compression or tension near the surface, moving further into compression with increased depth. The depth of the transition point from tension to compression also increased with increasing power density as shown in Table III.

Table III.

Effect of laser power density on the position of the transition from surface tension to subsurface compression residual stress

Laser power density / GW cm^{-2}	Depth of transition point / μm
0.5	80
1	95
3	145
4	320

The effects of ablative tape and damping were all studied with a power density of 1.0 GW/cm^2. Removing damping appeared to have little effect on the subsurface distribution of stresses, but surface stresses were moved further into tension, increasing the surface tension stress from 30-50 MPa to 75 MPa. Removing the ablative layers altogether and treating with just the damping present increased both the surface stresses (increased to 100-130 MPa tension), and increased the subsurface compressive stress from –50 to –100 MPa, at the same location as before. Direct ablation had little measureable effect either at the near surface or subsurface fields.

3.3 High resolution synchrotron X-ray measurements of residual stress distribution within the peened array

Residual strains in a selected sample peened with a power density of 3 GW/cm^2 were measured using synchrotron X-rays at the ID31 beam line of the European Synchrotron Radiation Facility (ESRF), Grenoble. Synchrotron X-rays offer the advantage of fine volume resolution and rapid count times [32]. An incident beam aperture of 2 mm (perpendicular to the peen line) × 50 μm (parallel to the peen line) was used. The strain-free lattice parameter d_0 was evaluated by calculating the average value of the lattice parameter from a series of measurements through the thickness of the plate in a region distant from the peened area.

Measurements were obtained of the through-thickness variation in residual strain, however, it was observed that the point-to-point variation in the profile with position *along* the peened line was far greater than was expected.

This is illustrated in figures 9 and 10, for the strain component perpendicular to the peen line. A series of measurements were made, spanning two peen spots, at a fixed depth of ~180 μm below the peened surface (figure 9), plus some additional measurements within a single peen spot at depths of ~380 and 580 μm (figure 10). The results show that there is considerable oscillation of strain (and hence stress) along the peen line, for single peen coverage with 5% overlap between the peen spots. The compressive strains are at the overlap regions of the spots, with tensile strains measured at the spot centres. With a small peened area, oscillatory residual stresses have been reported previously, either entirely compressive [33] or, for a small peened region in titanium, showing tensile stress at the spot centres [12].

Figure 10 compares the residual strain changes with depth at the peen spot overlap and at the spot centre. Also shown is the same strain component perpendicular to the peen line as measured by hole drilling, data derived from figure 7a. It can be seen that the hole drilling depth profile contains stresses intermediate between the local strain measurements produced by the synchrotron X-rays at the overlap and at the spot centre. The difference in strain between the spot centre and overlap increases as the

surface is approached, conversely at depths in excess of 600 μm all three are tending towards a common value of zero strain.

These results have significant implications for the use of laser peening in thin sections. It is clear that a single peen coverage does not produce the desired residual stress field, and also that the difference in stress parallel and perpendicular to a line of peened spots means that for externally applied loadings perpendicular to the peen line, the peen process may produce very little benefit.

3.4 Fatigue

Peening treatments of 1.0 and 3.0 GW/cm^2, both performed with damping and ablative tape, were selected for treatment of the fatigue samples. A total of eight fatigue samples were peened, four treated at a power density of 1.0 GW/cm^2 and four with a power density of 3.0 GW/cm^2. For each treatment two samples were scribed after peening to 50 μm depth, and two samples to 150 μm depth. These results were compared with previously published [27] fatigue test data on unpeened samples scribed to identical depths, and with fatigue data on unpeened, unscribed samples.

The fatigue endurance results for the peened and unpeened scribed samples can be seen in table IV.

Table IV Fatigue endurance of scribed and peened samples

LSP Intensity / GW/cm^2	Scribe depth / μm	Fatigue life Sample 1	Fatigue life Sample 2	Mean Life Peened samples	Mean life* unpeened samples From [27]	% difference in life produced by peening
1	50	9.19×10^4	9.11×10^4	9.15×10^4	6.23×10^4	+47
1	150	2.22×10^4	2.23×10^4	2.22×10^4	1.87×10^4	+18
3	50	6.99×10^4	8.14×10^4	7.56×10^4	6.23×10^4	+21
3	150	1.59×10^4	1.79×10^4	1.69×10^4	1.87×10^4	−10

* Endurance of unpeened unscribed samples is 2-3 × 10^5 cycles [27]

It can be seen that the best improvement in performance is given by the 1.0 GW/cm^2 applied to the 50 μm deep scribes, which produces a 47% improvement in life. The 3.0 GW/cm^2 applied to the same scribes produces only a 21% improvement in life. The effect of peening on the more severe 150 μm scribes was less impressive, the 1.0 GW/cm^2 treatment producing an 18% improvement in life, whereas the 3 GW/cm^2 treatment applied to the 150 μm deep scribes resulted in a 10% reduction in life. These

results appear to be very consistent: variability in measured life for each pair of samples tested in each condition being at its greatest ±6%, so the trends observed can be regarded with confidence. In the case of the 150 μm scribe with 3 GW/cm^2 peening, both the tested samples had reduced life compared with the mean life of the unpeened samples. Optical observations on the fracture surfaces confirmed that in all the samples the fatigue cracks initiated at the scribe roots and propagated across the sheet thickness. Rapid fracture occurred at crack lengths of about 500 μm.

Figure 11 shows the fracture surface of the sheets with a 50 μm deep scribe with peening treatment of 3 GW/cm^2. It can be seen that crack growth has occurred in a series of thumbnails. The distance between the points of maximum depth of the thumbnails was 5 mm, and the edges of the thumbnail corresponded to the overlap region of the peening pattern. Similar observations were made on the samples with 150 μm scribes and those peened at 1 GW/cm^2. This pattern matches the residual stress distribution shown in figure 9, corresponding to retardation of the crack at the edge of the peened area where the residual stresses are most compressive, with higher growth rates from the centre of the peened spot. Figure 12 shows an SEM picture of the fatigue crack originating from the scribe root and propagating for about 100 μm before final failure via void coalescence occurs.

4 Discussion

(a) Surface relief and hardness changes

The observations of surface relief associated with the laser peening treatment surprisingly do not appear to have been noted in previous published research; hardness observations are consistent with previous research. The total depth of the recess associated with the peen spot array is of the order of 30 μm, there being a local surface height increase of 15 μm adjacent to the peen spot boundary as well as a 15-μm-deep recess beneath the original sample surface. This suggests that at least some redistribution of material has occurred. From the dimensions of features in figure 5b, the end cross section of the rectangular recess is 15 μm × 6,000 μm = 9×10^4 μm^2, and the cross section of the two triangular areas of height increase on each side of the peen area is $2 \times 0.5 \times 15 \times 3{,}000 = 4.5 \times 10^4$ μm^2. Hence the area of height increase is approximately half that of the area of the recess, suggesting that both material removal and redistribution has occurred. Figures 5 a & b both show that within the recessed region the areas of peen spot overlap are of greater height than the centre of the peen spot areas which are at the lowest points of the recess. This observation also suggests that both material removal and redistribution have occurred during the peen spot formation event.

The microhardness contours in figure 6 are irregular, with both local maxima of 150 Hv and minima of 130 Hv occurring on the floor of the recessed area of the peen spot array. There are no obvious correlations of hardness with the overlap regions shown in figure 5b. The elevated regions in figure 5b on either side of the peen spot array are generally of hardness 135 with local variations of ±5 Hv, whereas regions in the recessed peen

spot array are generally harder (145 Hv), again with local variations of ±5 Hv. The hardness changes may be attributed to plastic deformation occasioned by the laser peen action.

(b) Residual stress fields

The residual stress fields developed by the peening process have stresses perpendicular to the peen line (σ_2) significantly more tensile (by 50-100 MPa) than those parallel to it (σ_1). For example power densities of 3 GW/cm^2 produced a maximum compressive σ_2 stress of –50 MPa, compared with –150 MPa compression parallel to the peen spot line. This stress asymmetry occurred on the surface and at all depths beneath the surface. Changes in laser power density changed the profile of residual stresses beneath the surface, but the stress perpendicular to the line was always more tensile than the one parallel to the peen line (see figure 7a, for example). Within 100 μm of the surface the σ_2 stress perpendicular to the peen line often became tensile; compression stresses that would inhibit fatigue occurred only at depths greater than this. There was little difference in the stress field developed in clad and in unclad samples as a comparison of figure 7a with 7b shows.

Measurements of residual strains at the improved spatial resolution provided by synchrotron X-rays show that at a depth of 180 μm the 0.25 mm wide peen spot overlaps are associated with local high compressive strains up to 1550 με, while regions in the peen spot centre are occupied by local tensile strains in the σ_2 direction perpendicular to the peen line of up to 1450 με (figure 12). Figure 10 suggests that at depths <180μm residual strains at both locations increase as the surface is approached; while at increasing depths they decline. At depths > 380 μm strains measured both by hole drilling and by synchrotron X-rays tend towards zero. Strains measured by hole drilling at the peen spot centre are smaller than those measured using synchrotron X-rays.

The differences between the residual strains measured by the two techniques may be a consequence of their different effective gauge volumes, as well as the positioning of the hole centre within the peen spot. Figure 13 shows schematically the positions of the peen spot overlap regions and the hole positions in relation to the strain contours measured using synchrotron X-rays. The 2 mm hole centre is located at the peen spot centre (position 2.5, 2.5). The hole area does not overlap the region of compression strain, and only partially covers the region of greatest tensile stress. Hence the residual strain value recorded by hole drilling will be biased towards tension and with a lower maximum than that recorded by the synchrotron X-rays, without sampling the near-surface compression strain region at the overlaps at all. Further confirmation of this view is provided by data from additional hole drilling experiments where the hole centre was located away from the peen spot centre towards the peen spot corner. Residual stress fields shifted towards compression relative to those recorded by hole drilling at the peen centre were recorded.

It was not possible to establish whether the stress asymmetry between σ_1 and σ_3 stresses recorded by hole drilling was reproducible using the higher resolution synchrotron X-ray method. Synchrotron X-ray measurements of strains parallel to the peen line (σ_1) were not taken owing to time constraints of the available beam time.

The observation that overlap regions are associated with compressive residual stress fields has been made previously, e.g. [12, 13]. Increasing the level of overlap from the 5% used in this work to 50% or even 100% can be predicted to move the stress field further towards compression and suggests that large numbers of multiple rows may not be needed to generate significant compressive residual stress fields – repeat coverage of a single row would have the same effect, with perhaps just 2 or 3 peening rows being all that is required.

The effect of increased laser power density was to increase the maximum compression achieved sub-surface and at the same time to move the location at which the maximum stress occurred to greater depths. Once again these effects are consistent with previous model predictions and experimental data [7-9, 13], made on much thicker samples in materials other than aluminium; hence the behaviour appears to be qualitatively generic – applicable to a range of materials and thicknesses.

The elastic stress concentrations K_t of the scribed notches are 9 for the 50 μm deep scribe and 14 for the 150 μm scribe [27]. Figure 7a shows that at 50 μm depth the residual stress orthogonal to the peen line is 35 MPa tension, and at 150 μm is 25 MPa compression, measured before the notch was cut. Applying the relevant K_t values to these stress values at the 50 μm notch root gives a stress of 315 MPa, and at the 150 μm notch root gives 350 MPa. Hence there is unlikely to be notch root yielding caused by residual stresses responding to the stress concentration as the elastic limit of 350 MPa for 2024 aluminium has not been exceeded. There will be some redistribution of the measured stress field caused by the cutting of the notch, as stressed material occupied by the notch volume will be removed and remaining stresses, which were in balance, must be redistributed. For scribes of this size this effect is thought to be small. The work of Jozelich [34], performing FE modelling of elastic stress fields ahead of V notches, shows that the region ahead of the notch root in which the stress field is modified will extend 10-15 microns ahead of the notch tip, before resuming the unnotched profile of figure 7a.

Effect of residual stresses on fatigue crack initiation and growth

In the present fatigue experiments, there were two peening treatments applied, 1 GW/cm^2 and 3 GW/cm^2, and two notch depths of 50 and 150 μm. The fatigue life changes produced by the laser peening range from almost 50% improvement for a 50 μm scribe subjected to peening of 1 GW/cm^2, to 10% life reduction for a 150 μm scribe subjected to 3 GW/cm^2. The best improvements are found for the 50 μm scribes and least for the 150 μm ones. Similarly the 1.0 GW/cm^2 treatments give greater improvements than the 3 GW/cm^2. Final failure crack lengths in peened samples were 400-500 μm – significantly smaller than those measured in unpeened samples [27].

The residual stress changes with depth for 1 and 3 GW/cm^2 treatments measured by hole drilling are shown in figure 14. It can be seen that at the tip of the 50 μm scribe both stress fields are 35-45 MPa tension; at the tip of the deeper 150 μm deep scribe, both fields are compressive with the 1 GW/cm^2 having –40 MPa, and the 3 GW/cm^2

having –20 MPa. For the scribe geometries used in the present research, Cini [27] has shown that cycles occupied in growing the fatigue crack from 50 μm to a failure crack length of 1 mm occupied 20-25 % of the total life, hence crack growth is a significant but lesser part of the total life in the absence of compressive residual stress fields such as those introduced by peening.

The application of the residual stress intensity concept (K_{resid}) [35-39] to models for fatigue crack growth has permitted accurate calculations of changes in fatigue crack growth rates and life caused by the presence of residual stresses from welds and other fabrication processes. Most influentially, residual compression stresses act to move the effective R ratio, R_{eff}, from positive to negative values, increasing crack closure and reducing the effective stress intensity range ΔK_{eff}. In turn the crack growth life will be greatly extended – to infinite values if the compression stress is great enough and $\Delta K_{eff} < \Delta K_{th}$ the threshold stress intensity range for crack growth. Tensile residual stresses will act in the reverse direction, increasing crack growth rates and reducing the overall life. Compressive residual stresses will also influence initiation behaviour; currently the extent and mechanism for this are not well understood.

To assess quantitatively the influence of laser peen residual stresses on crack growth lives in these samples, K_{resid} values as a function of crack depth were computed for the residual stress fields for 1 and 3 GW/cm^2 shown in figure 14. Together with the values of K_{max} and K_{min} applied via the external loading cycle, K_{resid} values were used to calculate changes in R_{eff} with crack depth using the expression.

$$R_{eff} = \frac{K_{min} + K_{resid}}{K_{max} + K_{resid}} \qquad (2)$$

In turn R_{eff} values were used to derive the ΔK_{eff} as a function of crack depth for each residual stress field, using the expressions quoted by Newman [40]. K_{resid} values were determined using a 2D finite element model created in ABAQUS. Linear elastic material properties with plane strain elements were used. The initial residual stress field σ_2 was incorporated into the model using the SIGINI sub routine. Stress intensities arising from the residual stress field were calculated using the Virtual Crack Closure Technique (VCCT) [41]. Crack growth was modelled by releasing individual nodes along the crack path, resulting in a redistribution of residual stress which in turn will modify the value of K_{resid} calculated at that crack depth.

For the stress fields from both the 1 and 3 GW/cm^2 treatments, K_{resid} values start at small (positive) tensile values at 50 μm depth and become negative (compression) first with the 1 GW/cm^2 field at 150 μm deep, and then the 3 GW/cm^2 at a depth of 200 μm. At greater depths K_{resid} values for 3 GW/cm^2 become more negative than those for 1 GW/cm^2.

There is little difference in the R_{eff} of the two peening treatments with increasing depth, up to a depth of 220 μm. R_{eff} values in both peening treatments decline together from 0.27 to 0.1, the externally imposed R ratio. At depths greater than 220 μm the R_{eff} is less than the externally imposed R = 0.1, but always remains positive, with R_{eff} of the 3 GW/cm^2 being less than the 1 GW/cm^2. Using the equations proposed originally by Newman [40] relating R to ΔK_{eff} for long fatigue cracks, the changes in ΔK_{eff} with depth can be seen in figure 15. There is little difference in the ΔK_{eff} values of the two

treatments, and no difference in fatigue crack growth rates and crack growth lives would be predicted.

Thus simple models based on residual stress intensities arising from measured residual stress fields do not account for the superiority of 1 GW/cm^2 peening treatments over that of 3 GW/cm^2, or of greater life improvement at 50 μm scribes compared with 150 μm scribes. It is likely that the equations [40] used to calculate ΔK_{eff} from R_{eff} derived for long cracks are not appropriate for these cracks of 50-400 μm depth. However the fine scale changes in residual stress field across the peen spots make it unlikely that the residual stress fields measured by hole drilling adequately represent local changes in K_{resid} in these samples.

The synchrotron X-ray measurements of residual stress show that at a finer scale than is measured by hole drilling, both positive and negative residual stresses exist within the peened area at a given depth. Fatigue cracks will initiate first in regions of tensile residual stress, and be inhibited in propagating in regions of compression. Figure 11 demonstrates the effect on crack development of the regions of compression and tension residual stress. Quantitative calculation of fatigue lives with regions of both tension and compression residual stress present will require 2D rather than 1D crack development models and is outside the scope of the present paper.

Conclusions

1. Residual stress measurements and fatigue life data have been obtained for 2-mm-thick 2024 T351 aluminium plates subjected to laser peening of intensities between 0.5 and 4 GW/cm^2.

2. Single coverage laser peening was used, in a localized region of the samples surrounding scribed notches 50-150 μm deep. There was 5% overlap between successive peen spots. Residual stresses measured using hole drilling were not equi-biaxial, and the residual stress component parallel to the peened line was always more compressive than that perpendicular to the peened line. Residual stresses orthogonal to the peen line at the surface were tensile, moving into compression at depths > 100-150 μm.

3. It was found that varying the peen intensity from 0.5 GW/cm^2 to 3 GW/cm^2 progressively increased the maximum compressive stress and moved the peak stress deeper into the body of the sheet.

4. Using synchrotron X-ray diffraction it was seen that the residual strains oscillated markedly along the peen line, with the tensile strains in the centre of the peen spot and high compression in the small overlap region. This strain pattern was corroborated by the profile of the fatigue cracks observed in the samples, which grew in a series of thumbnail profiles of period identical to the period of the strain oscillation. This behaviour is consistent with cracks initiating at regions of maximum tensile strain, and crack growth being inhibited in regions of compression.

5. A peen intensity of 1 GW/cm^2 was found to give an overall improvement in fatigue life with starter scribes of 50 and 150 μm depth, whereas for 3 GW/cm^2 peening there was little improvement in life for 50 μm scribes and a slight decrease in life for the longer scribe.

6. In terms of selection of peen conditions for thin sections, care must be taken in not "overpeening", leading to a largely tensile field near the surface. The use of multiple peen coverage must also be considered.

Acknowledgements

Synchrotron X-ray diffraction experiments were performed at the European Synchrotron Radiation Facility, Grenoble, and we are grateful for the assistance of Dr Alex Evans on beam line ID31. Murat Acar is thanked for help with the experimental execution. Peening treatment was performed by MIC Ltd. MEF is supported by a grant through The Open University from The Lloyd's Register Educational Trust, an independent charity working to achieve advances in transportation, science, engineering and technology education, training and research worldwide for the benefit of all.

Figure captions

Figure 1: Laser spot raster morphology. The example shown represents an overlap of 5% on a single row.

Figure 2: (a) clad 2024 T351 section showing cladding on outer layers; (b) Grain structure of 2024 T351; section on L-T plane.

Figure 3 Fatigue test sample showing dog bone shape and dimensions in mm

Figure 4 Section through 50 micron deep diamond cut scribe.

Figure 5: (a) Optical view of the peened row on clad fatigue sample showing surface relief; and (b) Measured surface profile of three peened spots, peened at an intensity of 3 GW/cm^2. The axes are in mm.

Figure 6: Vickers hardness profile along the line of peened spots for 3 GW/cm^2 peen intensity. X and Y axes are in mm.

Figure 7: Residual stresses parallel and perpendicular to the peen line as a function of depth in two samples peened with 3 GW/cm^2 intensity: (a) with cladding (b) without cladding.

Figure 8: Effect of power density on maximum compressive residual stress, showing increasing compression peak with increasing power density up to 3 GW/cm^2.

Figure 9: Contour map of residual strain field perpendicular to the peen line at a depth of 180 μm for two complete 5 mm square peen spots within the linear array, overlapping by 0.2 mm. Regions of overlap along the peen line are at 1 mm, 6 mm and 11 mm. The spot centre lines are at 3.5 and 8.5 mm. Laser pulses 3.0 GW/cm^2

Figure 10: Comparison of depth profiles of residual strain perpendicular to the peen line produced by laser pulses of 3.0 GW/cm^2 as measured by hole drilling and as measured by synchrotron radiation at locations of overlap and at the peen centre.

Figure 11: Optical view of fracture surface produced by fatigue crack growth. 50 μm scribe on top edge of sample image; crack growth direction from top to bottom.

Figure 12: SEM picture of the fracture surface of fatigue sample treated with 3 GW/cm^2 with 50 micron scribe showing fatigue crack development from scribe root, growth for 100 μm followed by rapid failure via void coalescence.

Figure 13: Schematic diagram of residual stress contours within 2 peen spots adapted from figure 9, showing relation of strain field to overlap regions and to the location of the holes drilled to measure residual stress.

Figure 14: Comparison of residual stresses perpendicular to the peen line produced by 1 and by 3 GW/cm^2 laser peen treatments.

Figure 15: Plot of ΔK_{eff} changes with crack depth for 1 and for 3 GW/cm^2 peening treatments.

References

[1] Q. Liu, C. H. Yang, K. Ding, S. A. Barter and L. Ye, The effect of laser power density on the fatigue life of laser-shock-peened 7050 aluminium alloy, Fatigue & Fracture Of Engineering Materials & Structures. 30 (2007) 1110-1124.
[2] Y. Cao, Y. C. Shin and B. Wu, Parametric Study on Single Shot and Overlapping Laser Shock Peening on Various Metals via Modeling and Experiments, Journal of Manufacturing Science and Engineering. 132 (2010) 061010-061010.
[3] Y. Ochi, T. Matsumura, T. Ikarashi, K. Masaki, T. Kakiuchi, Y. Sano and T. Adachi, Effects of laser peening treatment without protective coating on axial fatigue property of aluminum alloy, Procedia Engineering. 2 (2010) 491-498.
[4] C. Rubio-Gonzalez, J. L. Ocana, G. Gomez-Rosas, C. Molpeceres, M. Paredes, A. Banderas, J. Porro and M. Morales, Effect of laser shock processing on fatigue crack growth and fracture toughness of 6061-T6 aluminum alloy, Materials Science and Engineering A. 386 (2004) 291-295.
[5] X. Ling, W. Peng and G. Ma, Influence of Laser Peening Parameters on Residual Stress Field of 304 Stainless Steel, Journal of Pressure Vessel Technology. 130 (2008) 021201-021208.
[6] J. E. Rankin, M. R. Hill and L. A. Hackel, The effects of process variations on residual stress in laser peened 7049 T73 aluminum alloy, Materials Science and Engineering A. 349 (2003) 279-291.
[7] X. C. Zhang, Y. K. Zhang, J. Z. Lu, F. Z. Xuan, Z. D. Wang and S. T. Tu, Improvement of fatigue life of Ti-6Al-4V alloy by laser shock peening, Materials Science and Engineering: A. 527 (2010) 3411-3415.
[8] A. Chahardehi, F. P. Brennan and A. Steuwer, The effect of residual stresses arising from laser shock peening on fatigue crack growth, Engineering Fracture Mechanics. 77 (2010) 2033-2039.
[9] A. D. Evans, A. King, T. Pirling, P. Peyre and P. J. Withers, in S. Pantelakis and C. Rodopoulos (eds.), *Engineering Against Fracture*, Springer Netherlands, 2009, p. 383-398-398.
[10] J. Zhou, S. Huang, S. Jiang and Y. Fan, Numerical simulation on fatigue crack growth of metal sheet induced by laser shot peening, Intl J. Modern Phys. B. 23 (2009) 1646-1651.
[11] A. King, A. Steuwer, C. Woodward and P. J. Withers, Effects of fatigue and fretting on residual stresses introduced by laser shock peening, Materials Science and Engineering: A. 435-436 (2006) 12-18.
[12] R. A. Brockman, W. R. Braisted, S. E. Olson, R. D. Tenaglia, A. H. Clauer, K. Langer and M. J. Shepard, Prediction and characterization of residual stresses from laser shock peening, Int. J. Fatigue. 36 (2012) 96-108.
[13] G. Gomez-Rosas, C. Rubio-Gonzalez, J. L. OcaÒa, C. Molpeceres, J. A. Porro, W. Chi-Moreno and M. Morales, High level compressive residual stresses produced in aluminum alloys by laser shock processing, Applied Surface Science. 252 (2005) 883-887.
[14] O. Hatamleh, A comprehensive investigation on the effects of laser and shot peening on fatigue crack growth in friction stir welded AA 2195 joints, International Journal of Fatigue. 31 (2009) 974-988.

[15] O. Hatamleh, S. Forth and A. Reynolds, Fatigue Crack Growth of Peened Friction Stir-Welded 7075 Aluminum Alloy under Different Load Ratios, Journal of Materials Engineering and Performance. 19 (2010) 99-106-106.
[16] O. Hatamleh, J. E. D. Lyons and R. Forman, Laser peening and shot peening effects on fatigue life and surface roughness of friction stir welded 7075-T7351 aluminum, Fatigue & Fracture Of Engineering Materials & Structures. 30 (2007) 115-130.
[17] H. Luong and M. R. Hill, The effects of laser peening on high-cycle fatigue in 7085-T7651 aluminum alloy, Materials Science and Engineering: A. 477 (2008) 208-216.
[18] H. Luong and M. R. Hill, The effects of laser peening and shot peening on high cycle fatigue in 7050-T7451 aluminum alloy, Materials Science and Engineering: A. 527 (2010) 699-707.
[19] P. Peyre, R. Fabbro, P. Merrien and H. P. Lieurade, Laser shock processing of aluminium alloys. Application to high cycle fatigue behaviour, Materials Science and Engineering A. 210 (1996) 102-113.
[20] L. Zhang, K. Y. Luo, J. Z. Lu, Y. K. Zhang, F. Z. Dai and J. W. Zhong, Effects of laser shock processing with different shocked paths on mechanical properties of laser welded ANSI 304 stainless steel joint, Materials Science and Engineering: A. 528 (2011) 4652-4657.
[21] J. M. Yang, Y. C. Her, N. Han and A. Clauer, Laser shock peening on fatigue behavior of 2024-T3 Al alloy with fastener holes and stopholes, Materials Science and Engineering: A. 298 (2001) 296-299.
[22] K. Y. Luo, J. Z. Lu, L. F. Zhang, J. W. Zhong, H. B. Guan and X. M. Qian, The microstructural mechanism for mechanical property of LY2 aluminum alloy after laser shock processing, Materials & Design. 31 (2010) 2599-2603.
[23] Y. K. Zhang, J. Z. Lu, X. D. Ren, H. B. Yao and H. X. Yao, Effect of laser shock processing on the mechanical properties and fatigue lives of the turbojet engine blades manufactured by LY2 aluminum alloy, Materials and Design. 30 (2009) 1697-1703.
[24] J. Z. Lu, K. Y. Luo, Y. K. Zhang, G. F. Sun, Y. Y. Gu, J. Z. Zhou, X. D. Ren, X. C. Zhang, L. F. Zhang, K. M. Chen, C. Y. Cui, Y. F. Jiang, A. X. Feng and L. Zhang, Grain refinement mechanism of multiple laser shock processing impacts on ANSI 304 stainless steel, Acta Materialia. 58 (2010) 5354-5362.
[25] J. Z. Lu, K. Y. Luo, Y. K. Zhang, C. Y. Cui, G. F. Sun, J. Z. Zhou, L. Zhang, J. You, K. M. Chen and J. W. Zhong, Grain refinement of LY2 aluminum alloy induced by ultra-high plastic strain during multiple laser shock processing impacts, Acta Materialia. 58 (2010) 3984-3994.
[26] *The properties of aluminium and its alloys.* The Aluminium Federation, West Bromwich, UK, 1983.
[27] A. Cini and P. E. Irving, Transformation of defects into fatigue cracks; the role of Kt and defect scale on fatigue life of non-pristine components, Procedia Engineering. 2 (2010) 667-677.
[28] M. Dorman, MSc thesis Cranfield University, 2008.
[29] P. V. Grant, J. D. Lord and P. S. Whitehead, Measurement Good Practice Guide No. 53: The Measurement of Residual Stresses by the Incremental Hole Drilling Technique, National Physical Laboratory, 2002., Teddington, UK, 2002.
[30] G. S. Schajer, Measurement of Non-Uniform Residual Stresses Using the Hole Drilling Method, J. Engng Mater. Tech. . 110 (1988) 338-343.

[31] B. Clausen, T. Lorentzen and T. Leffers, Self-consistent modelling of the plastic deformation of f.c.c. polycrystals and its implications for diffraction measurements of internal stresses, Acta Materialia. 46 (1998) 3087-3098.
[32] C. Riekel, in M. E. Fitzpatrick and A.Lodini (eds.), *Analysis of Residual Stresses by Diffraction Using Neutron and Synchrotron Radiation*, Taylor & Francis, London, 2003, p. 28-44.
[33] X. D. Ren, Y. K. Zhang, H. F. Yongzhuo, L. Ruan, D. W. Jiang, T. Zhang and K. M. Chen, Effect of laser shock processing on the fatigue crack initiation and propagation of 7050-T7451 aluminum alloy, Materials Science and Engineering: A. 528 (2011) 2899-2903.
[34] A. M. Jozelich, 'Investigation of the transformation of defects into fatigue cracks', MSc Thesis, Cranfield University, 2009.

[35] G. Glinka, “Effect of residual stresses on fatigue crack growth in steel weldments under constant and variable amplitude loads” ASTM STP 677 (1979) pp 198-214.
[36] A. P. Parker, “Stress intensity factors, crack profiles and fatigue crack growth rates in residual stress fields”. ASTM STP 776, (1982) 13-31.
[37] M. Beghini, L. Bertini, Engng Fract. Mech. 36 (1990) 379-387.
[38] G. Pouget , A. P. Reynolds, Intl J. Fatigue 30 (2008) pp 463-472.
[39] G. Servetti, X. Zhang, Engng Fract. Mech. 76 (2009) 1589-1602.
[40] J. C. Newman, Intl J. Fracture 24 (1984) 131-135.
[41] R. Kruegar (2002) “The virtual crack closure technique: history approach and applications” NASA /CR-2002-211628; NASA.

Figure(1)

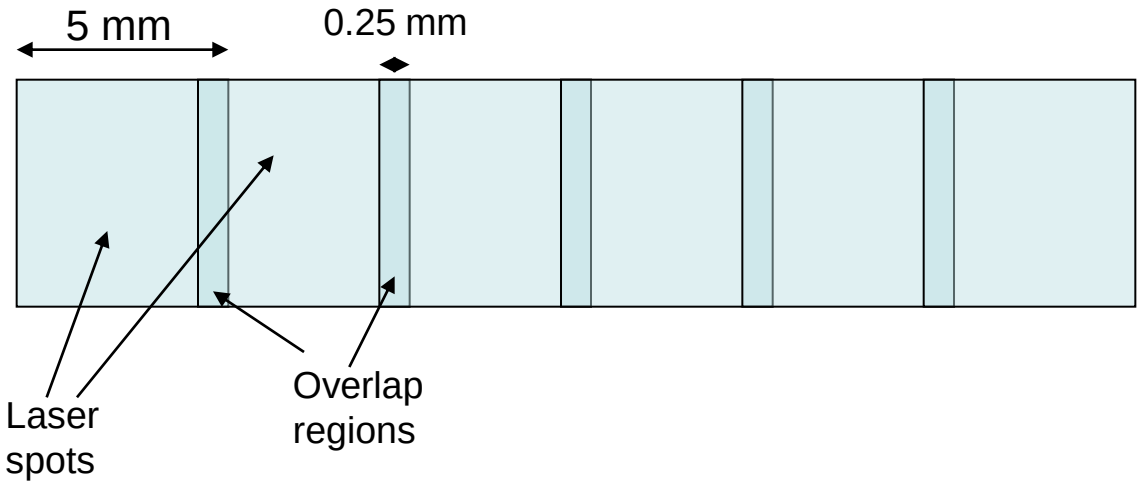

Figure 1: Laser spot raster morphology. The example shown represents an overlap of 5% on a single row.

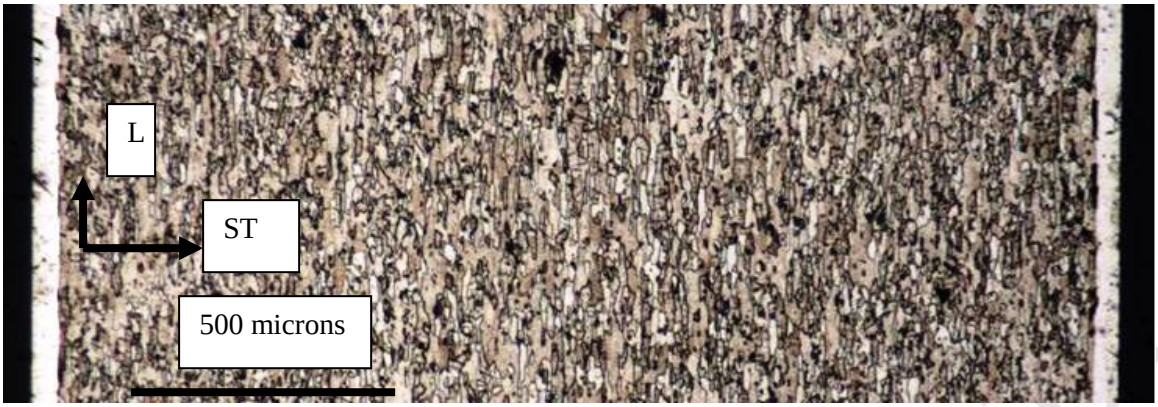

(2a)

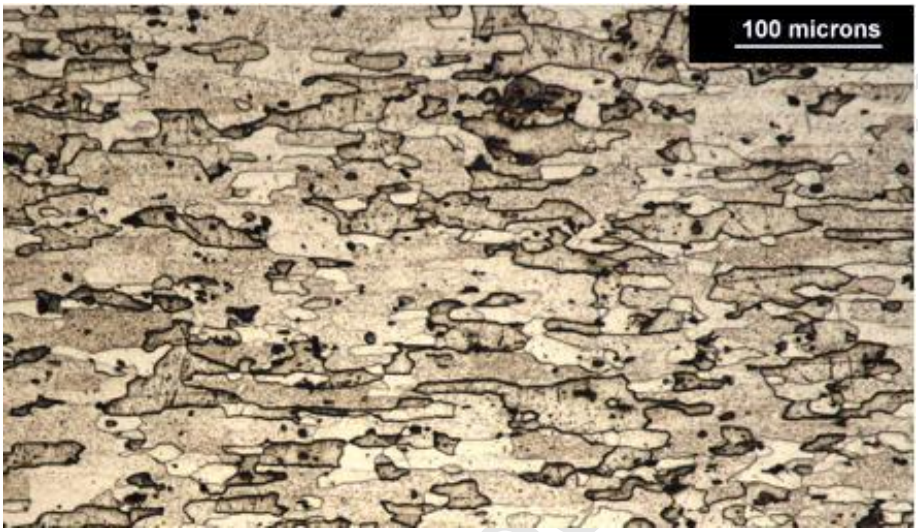

(2b)

Figure 2: (a) clad 2024 T351 section showing cladding on outer layers; (b) Grain structure of 2024 T351; section on L-ST plane.

Figure(3)

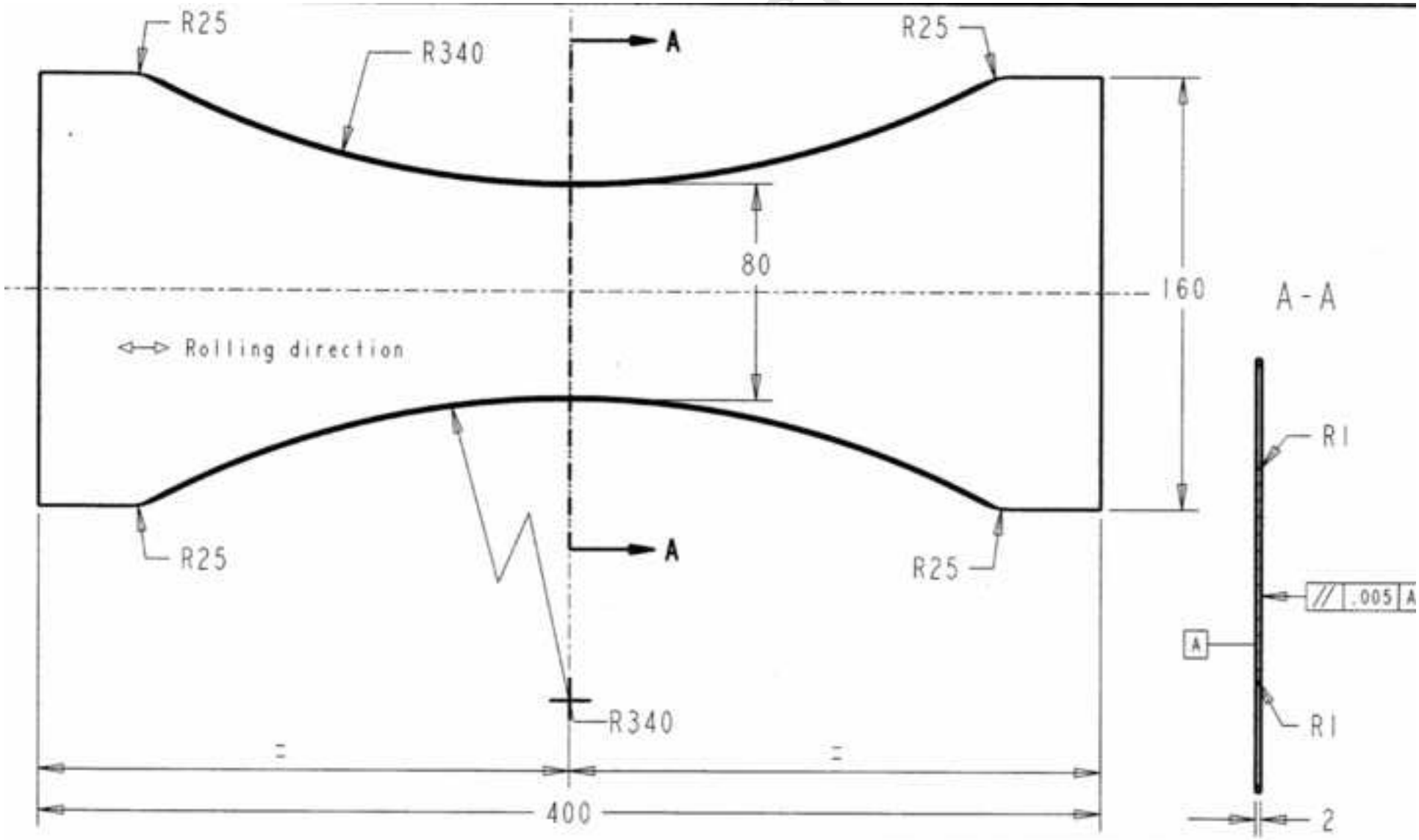

Figure 3 Test sample showing dog bone shape and dimensions in mm

Figure(4)

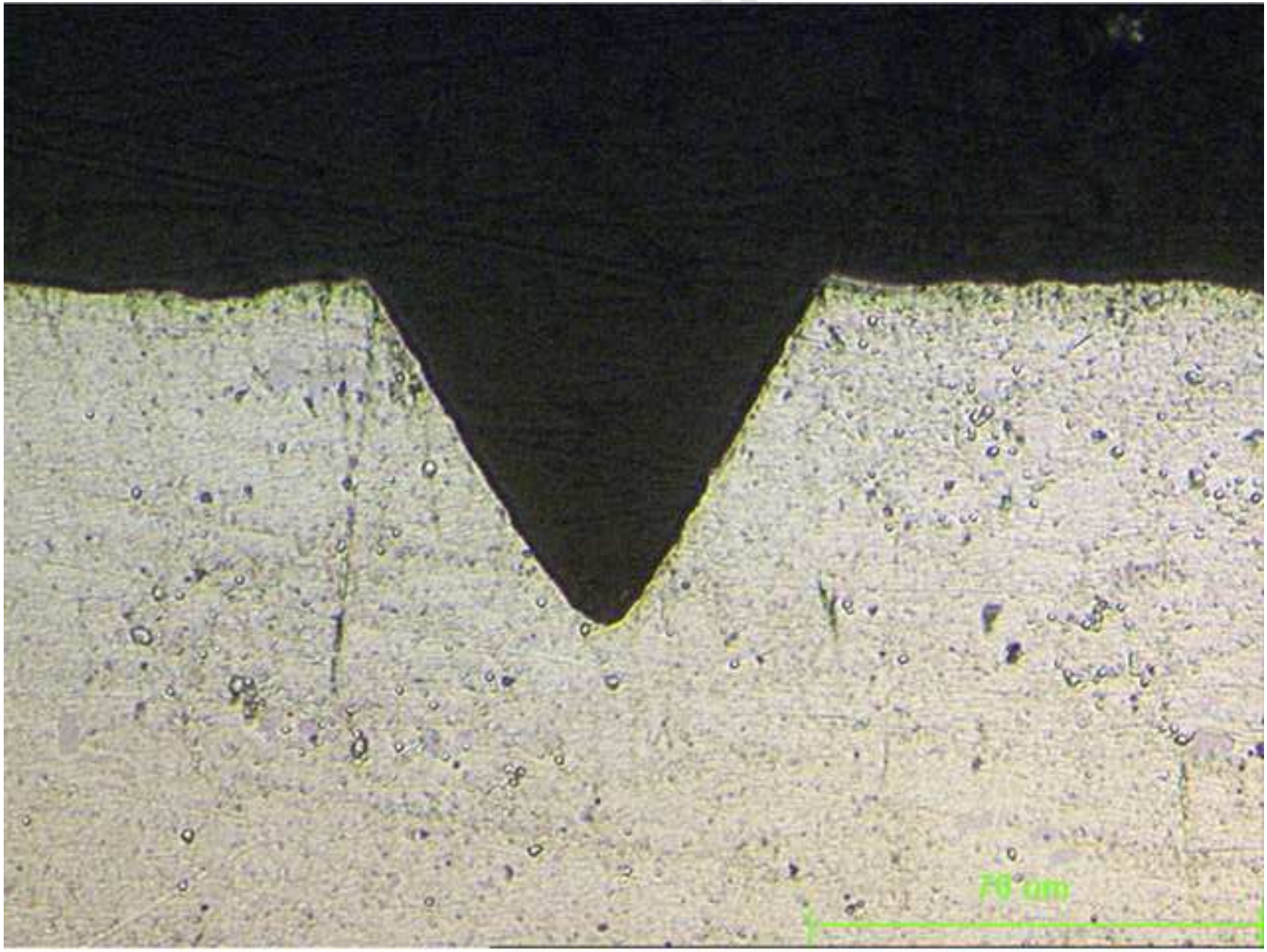

Figure 4 Section through 50 micron deep diamond cut scribe.

Figure(5a)

Figure 5: (a) Optical view of the peened row on clad fatigue sample showing surface relief;

Figure(5b)

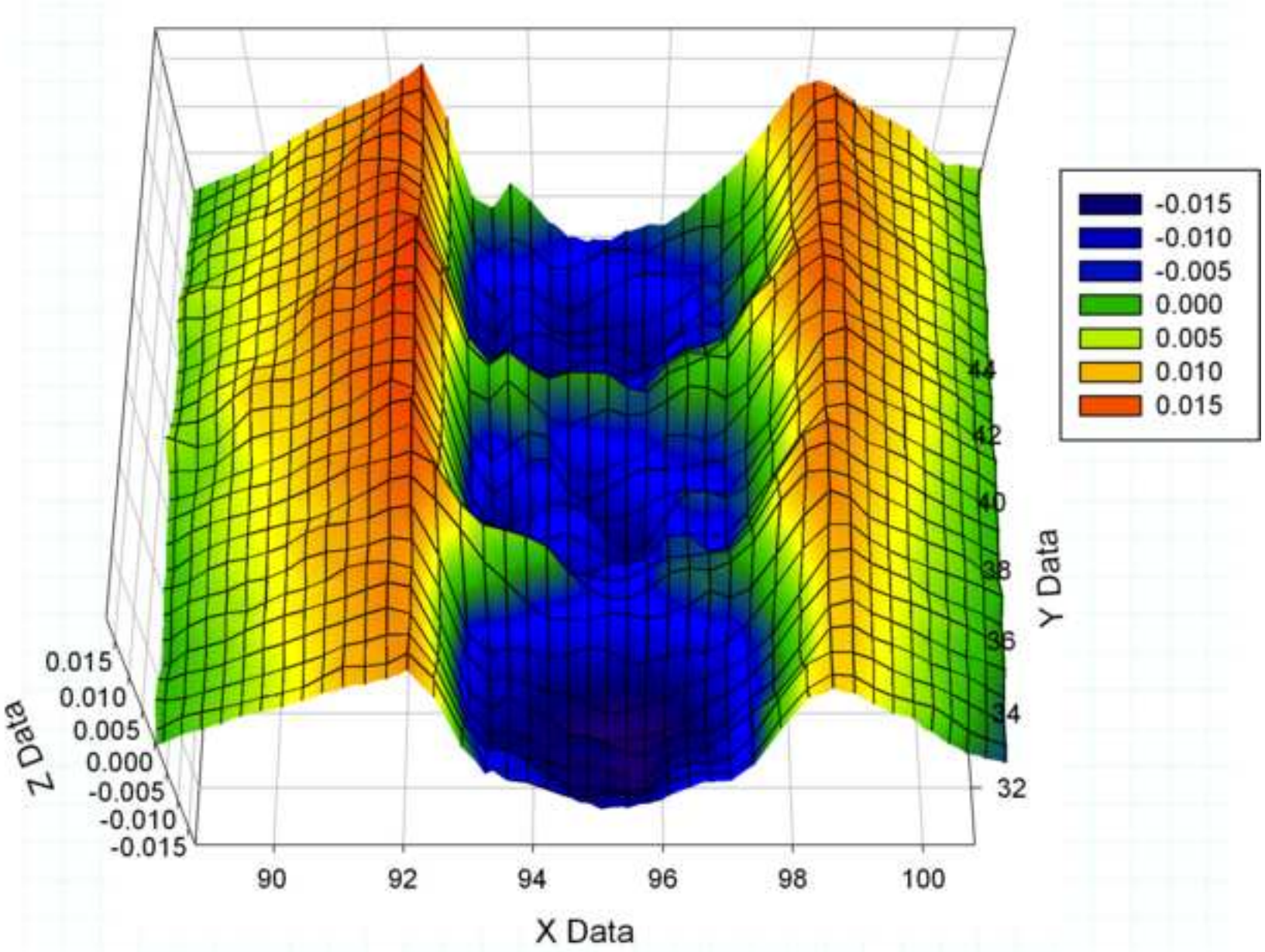

Figure 5(b) Measured surface profile of three peened spots, peened at an intensity of 3 GW/cm2. The axes are in mm.

Figure(6)

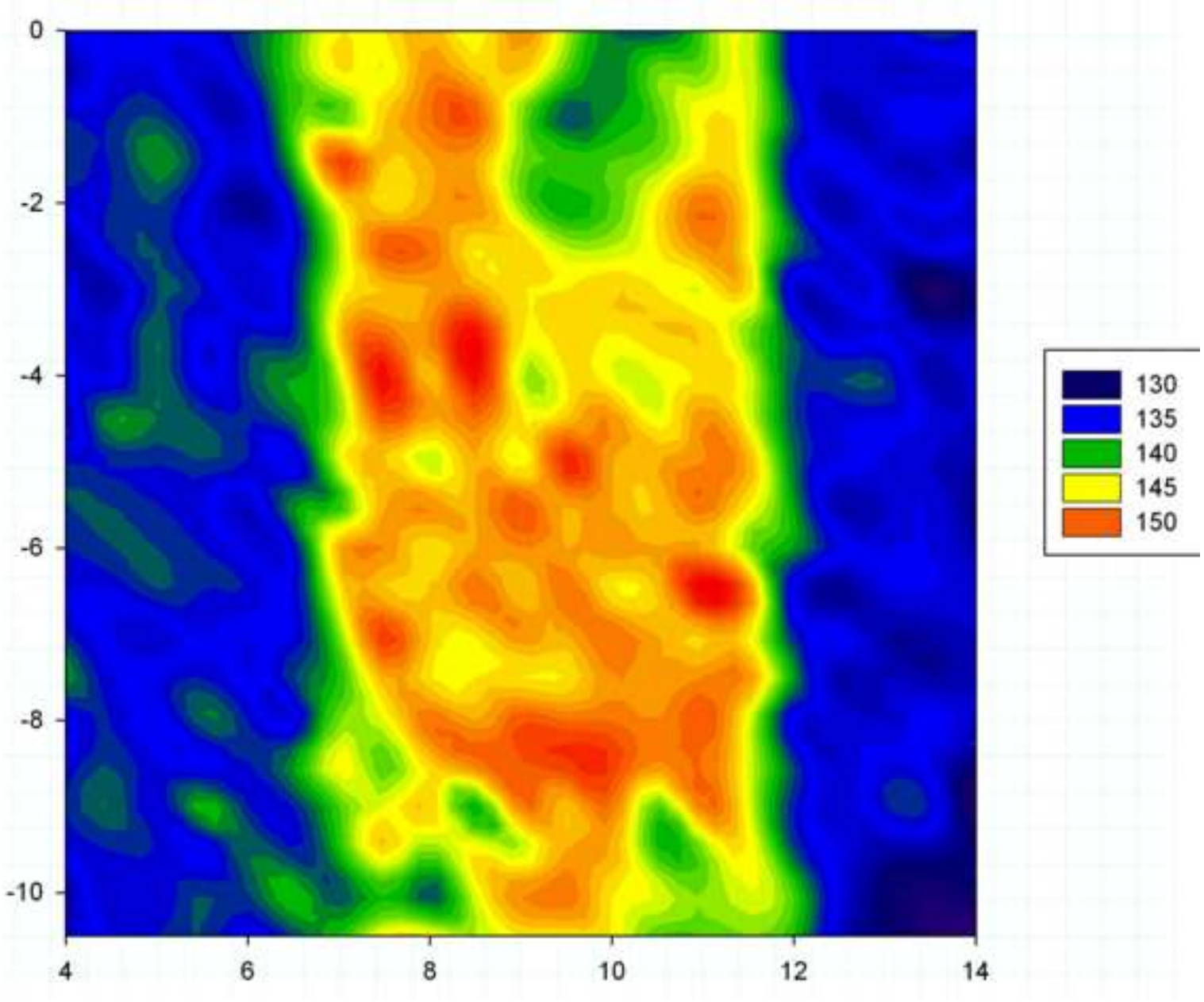

Figure 6: Vickers hardness profile along the line of peened spots for 3 GW/cm2 peen intensity. X and Y axes are in mm.

Figure(7a)

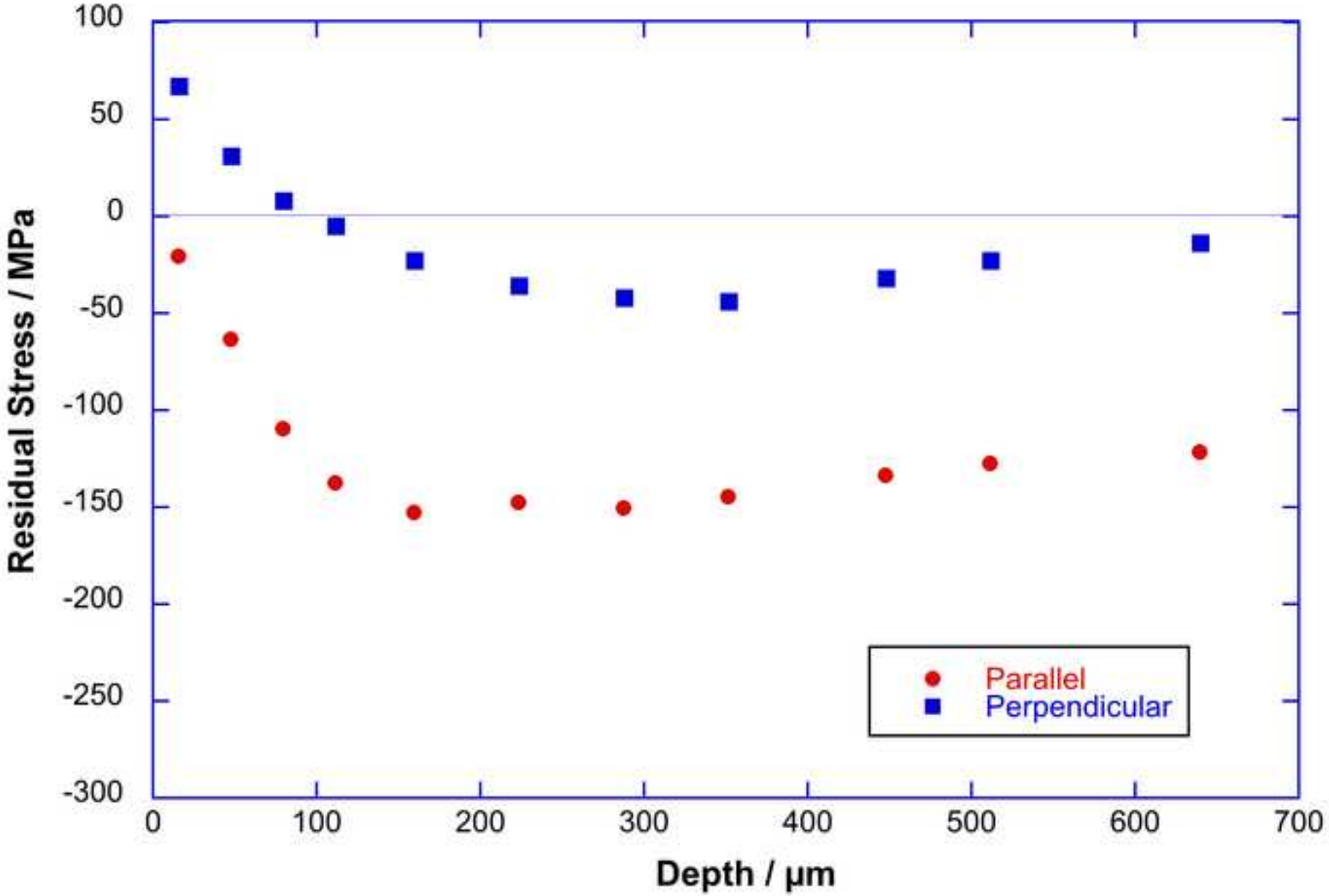

Figure 7: Residual stresses as a function of depth in two samples peened with 3 GW/cm2 intensity: (a) with cladding; □1 is parallel to the peened line, □2 is perpendicular to it.

Figure(7b)

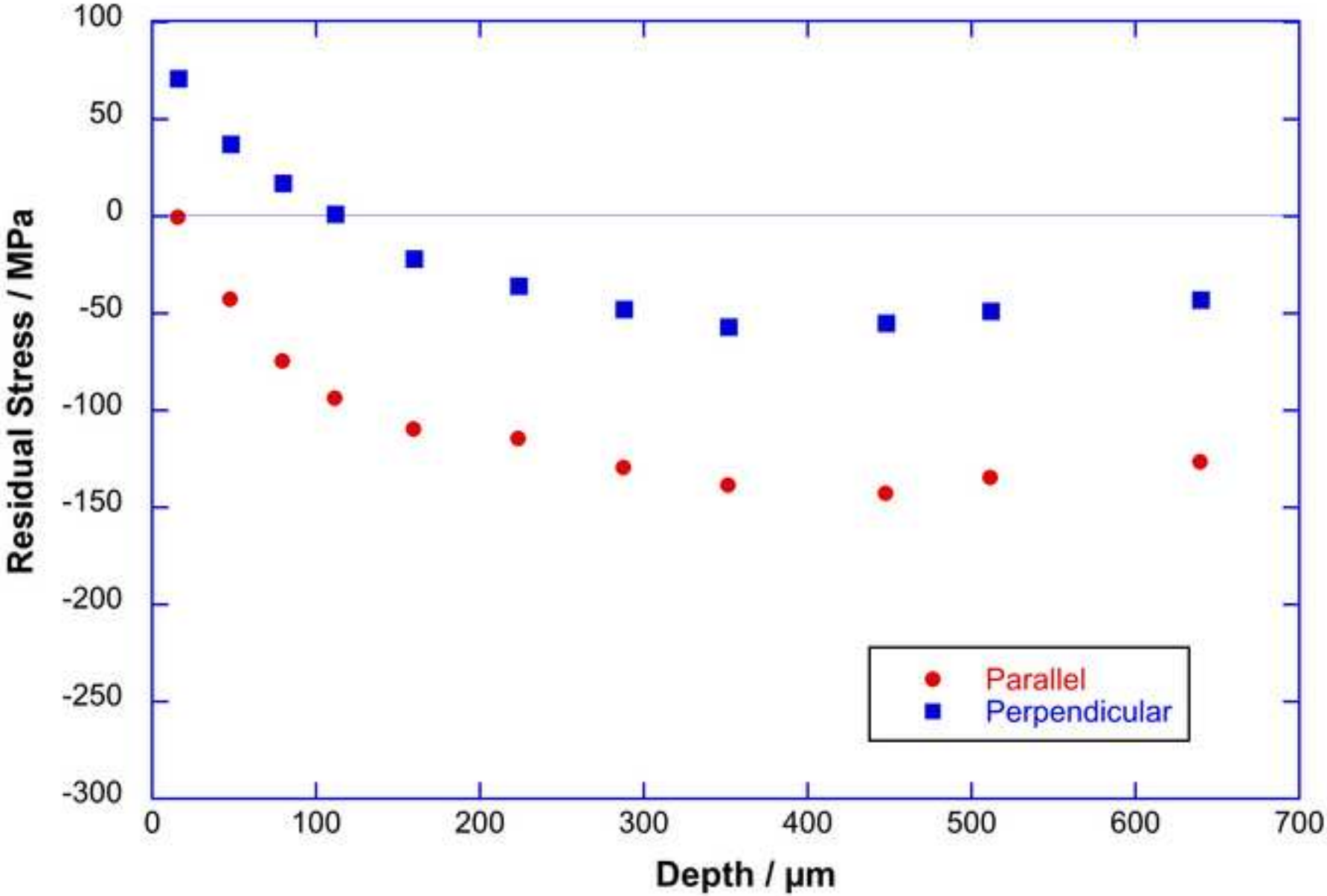

Figure 7: Residual stresses as a function of depth in two samples peened with 3 GW/cm2 intensity: (b) without cladding; □1 is parallel to the peened line, □2 is perpendicular to it.

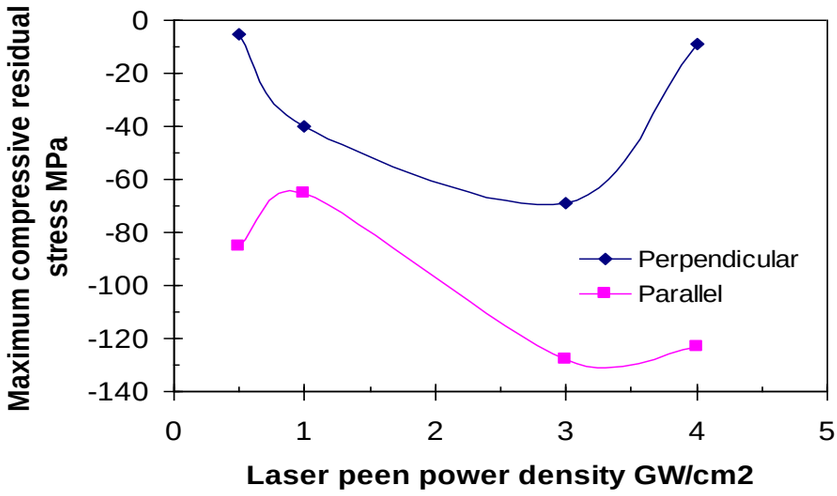

Figure 8: Effect of power density on maximum compressive residual stress, sho increasing compression peak with increasing power density up to 3 GW/cm^2.

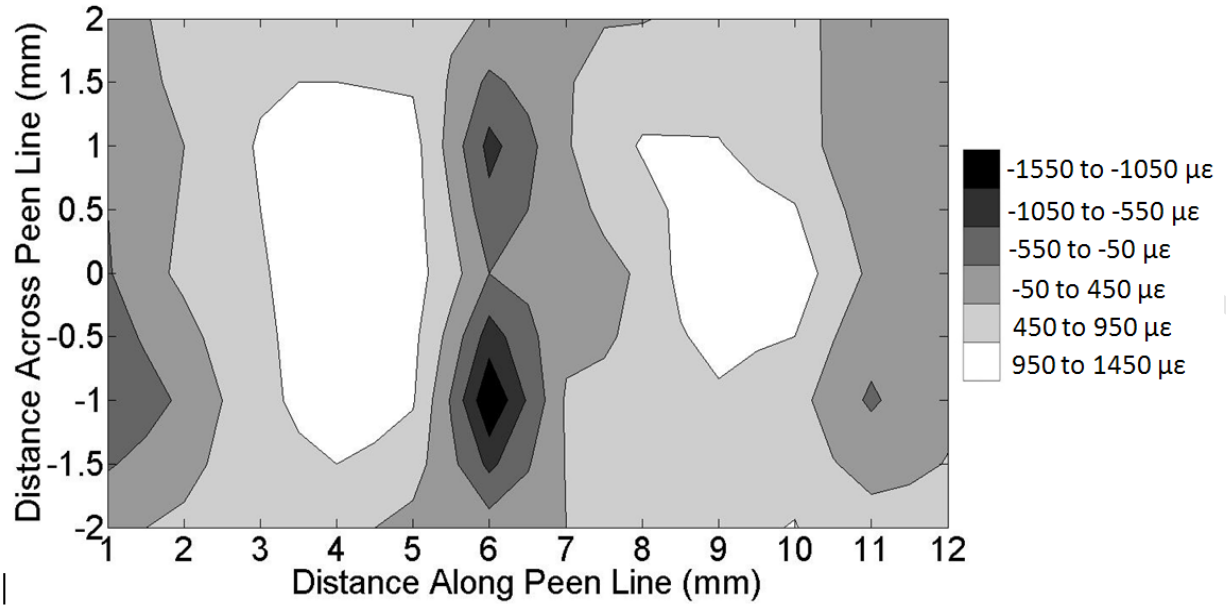

Figure 9: Contour map of residual strain field perpendicular to the peen line at a depth of 180 μm for two complete 5 mm square peen spots within the linear array, overlapping by 0.2 mm. Regions of overlap along the peen line are at 1mm, 6 mm and 11 mm. The spot centre lines are at 3.5 and 8.5 mm. Laser pulses 3.0 GW/cm$^{2.}$.

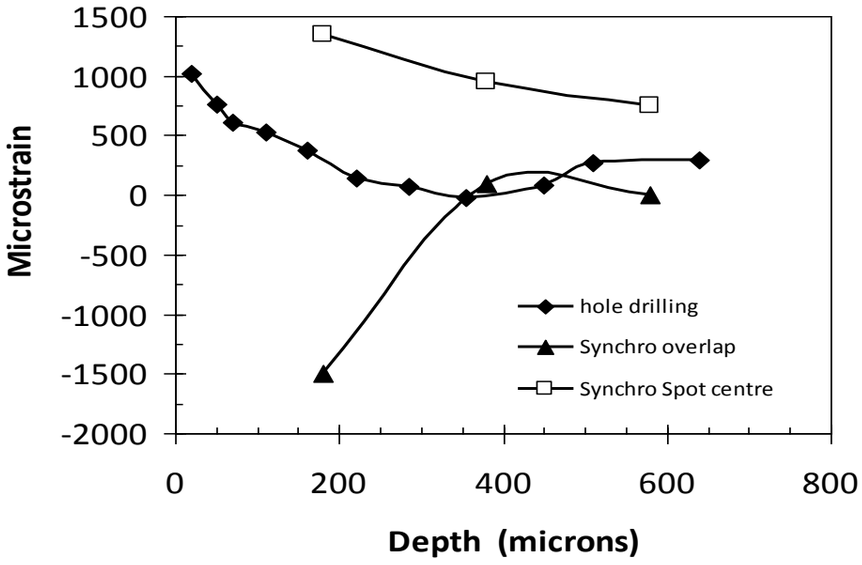

Figure 10 Comparison of depth profiles of residual strain perpendicular to the peen line produced by laser pulses of 3.0 GW/cm^2 as measured by hole drilling and as measured by synchrotron radiation at locations of overlap and at the peen centre.

Figure 13 Schematic diagram of residual stress contours within 2 peen spots adapted from figure 12, showing relation of strain field to overlap regions and to the location of the holes drilled to measure residual stress.

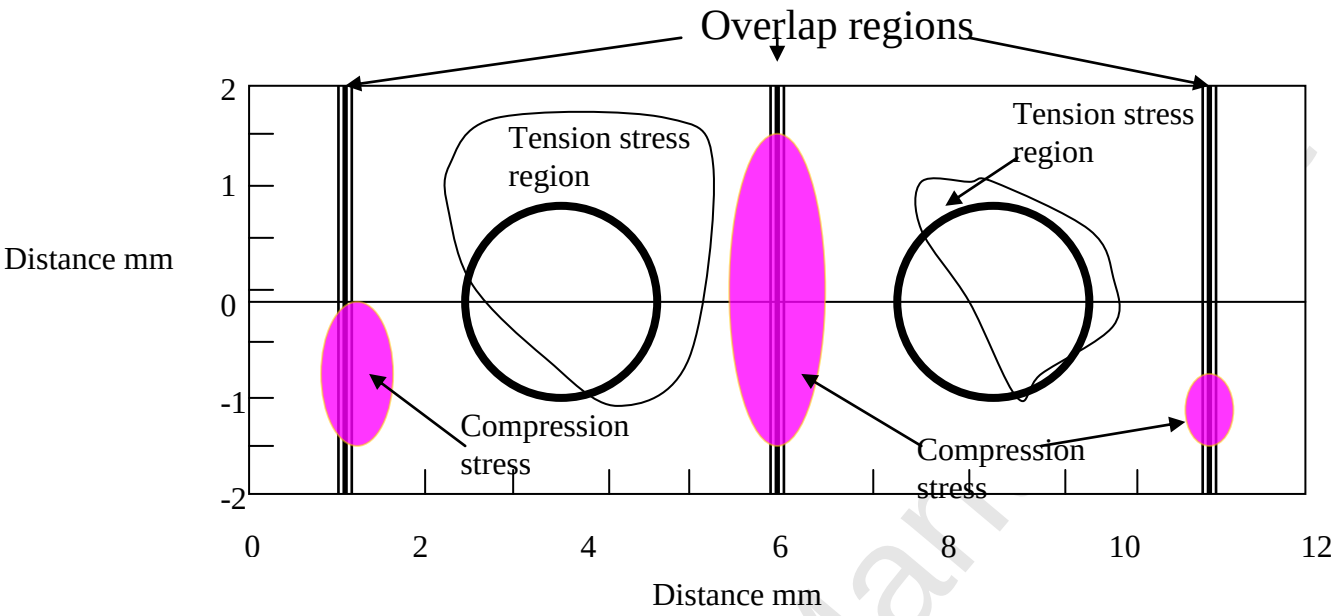

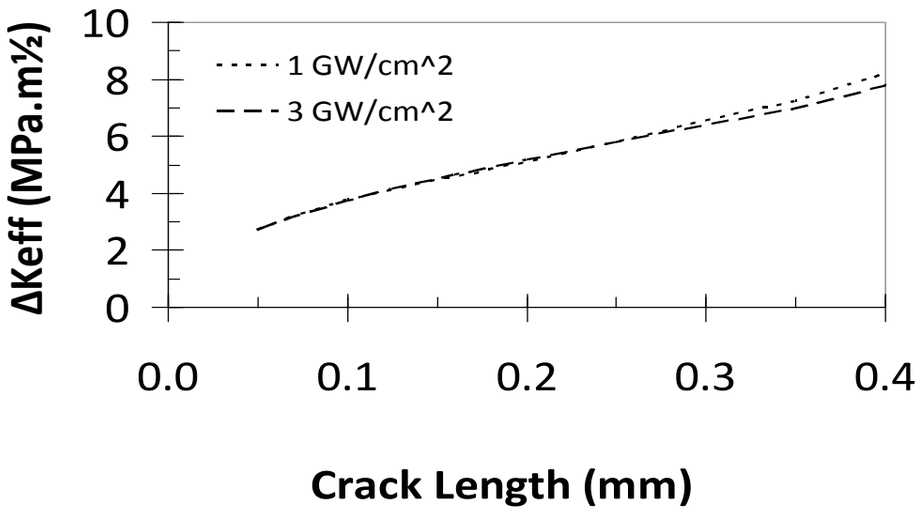

Figure 15 Plot of Δ K changes with crack depth for 1 and for 3 GW/cm2 peening treatments

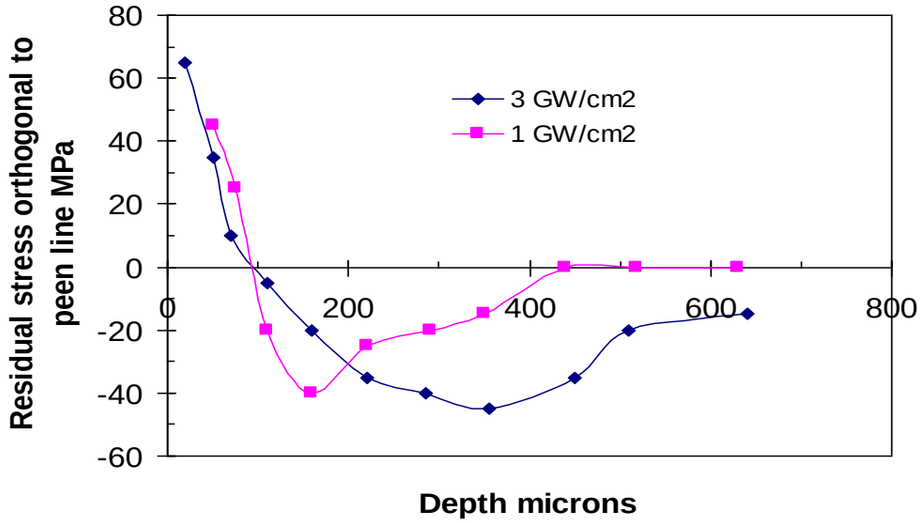

Figure 14 Comparison of stresses perpendicular to the peen line produced by 1 and by 3 GW/cm^2 laser peen treatments.

Figure(11)

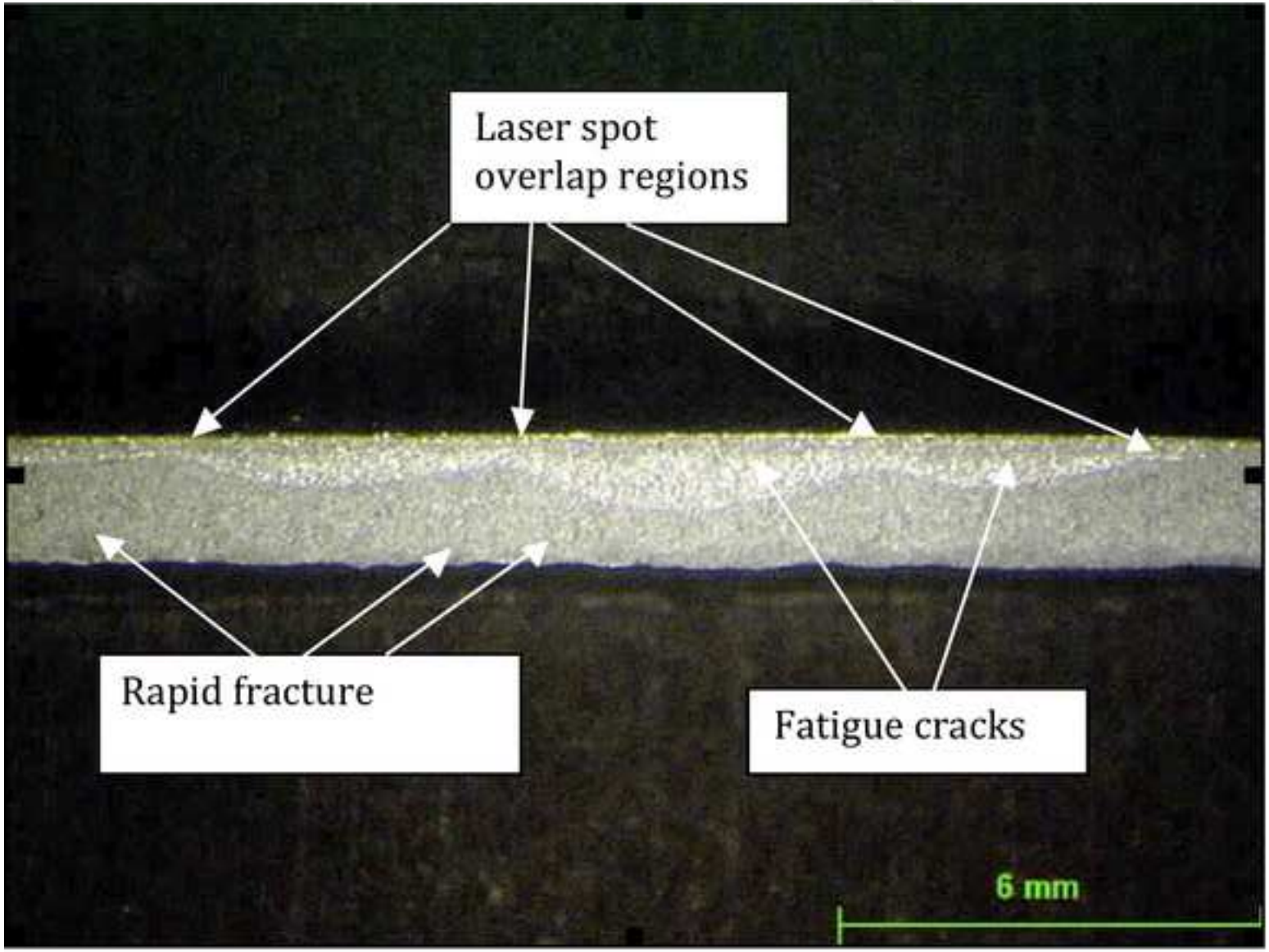

Figure 11

Optical view of fracture surface produced by fatigue crack growth. 50 μm scribe on top edge of sample image; crack growth direction from top to bottom.

Figure(12)

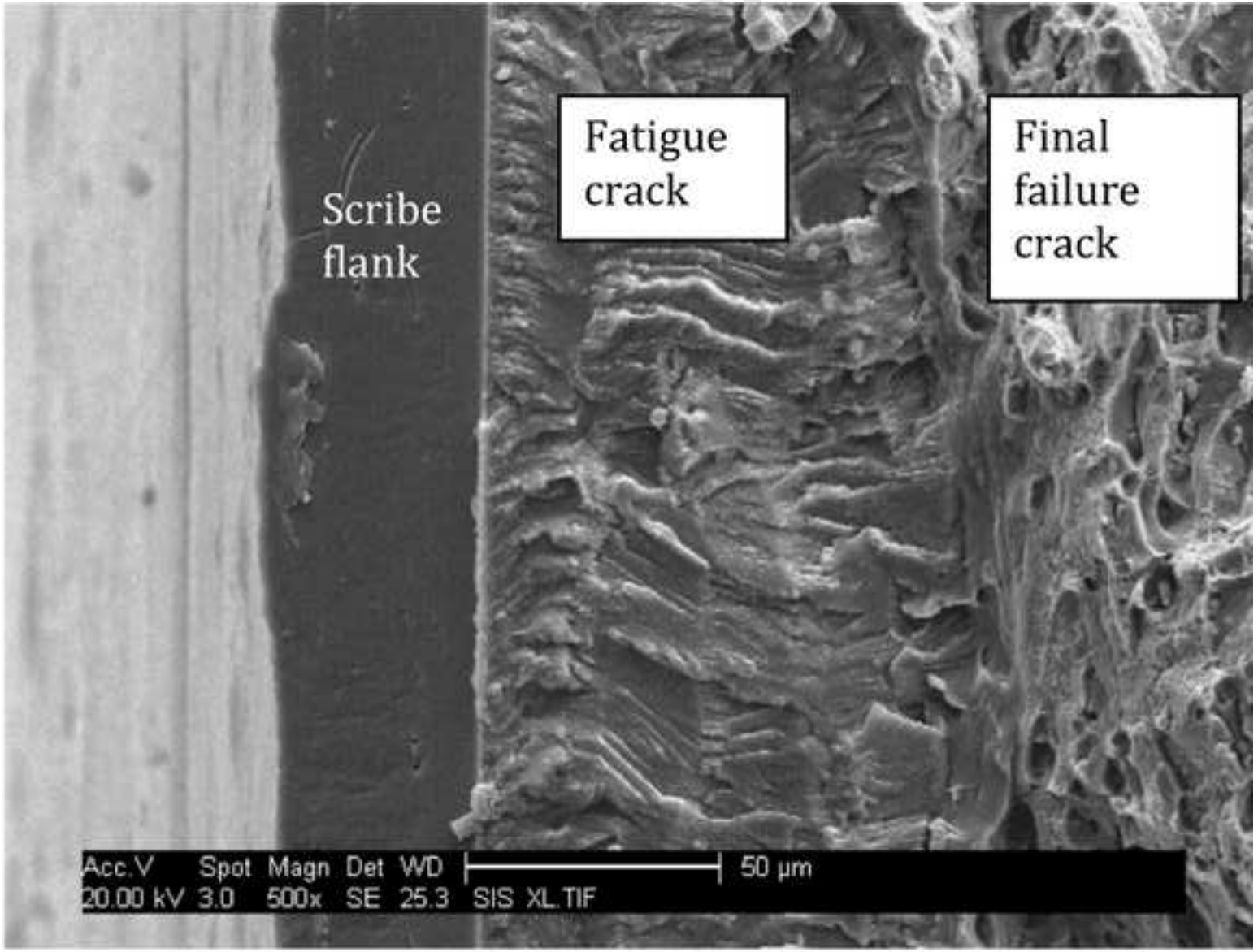

Figure 12 SEM picture of the fracture surface of fatigue sample treated with 3 GW/cm^2 with 50 micron scribe showing fatigue crack development from scribe root, growth for 100 µm followed by rapid failure via void coalescence.

Table I.

Typical mechanical properties of clad 2024 T351 [19]

Material	Young modulus E / MPa	Yield stress $\sigma_{0.2}$ / MPa	Ultimate stress σ_u / MPa	Elongation at fracture / %
Al 2024-T351	72000	360	481	19

Table II

Effect of laser power density on depth of compression maximum stress perpendicular to peen line

Laser power density / GW cm^{-2}	Depth of peak compressive stress / µm
0.5	100
1	180
3	315
4	450

Table III.

Effect of laser power density on the position of the transition from surface tension to subsurface compression residual stress

Laser power density / GW cm^{-2}	Depth of transition point / µm
0.5	80
1	95
3	145
4	320

Table IV

Fatigue endurance of scribed and peened samples

LSP Intensity / GW/cm^2	Scribe depth / μm	Fatigue life Sample 1	Fatigue life Sample 2	Mean Life Peened samples	Mean life* unpeened samples From [21]	% difference in life produced by peening
1	50	9.19×10^4	9.11×10^4	9.15×10^4	6.23×10^4	+47
1	150	2.22×10^4	2.23×10^4	2.22×10^4	1.87×10^4	+18
3	50	6.99×10^4	8.14×10^4	7.56×10^4	6.23×10^4	+21
3	150	1.59×10^4	1.79×10^4	1.69×10^4	1.87×10^4	–10

* Endurance of unpeened unscribed samples is 2-3 × 10^5 cycles [27]